Molecular-level speciation of Eu(III) adsorbed on a migmatized gneiss as determined using μTRLFS

Molodtsov, K.; Demnitz, M.; Schymura, S.; Jankovský, F.; Havlová, V.; Schmidt, M.;

Originally published:

April 2021

Environmental Science and Technology 55(2021)8, 4871-4879

DOI: https://doi.org/10.1021/acs.est.0c07998

Perma-Link to Publication Repository of HZDR:

https://www.hzdr.de/publications/Publ-32206

Molecular-level speciation of Eu(III) adsorbed on a migmatised gneiss as determined using µTRLFS

Konrad Molodtsov,[1] Maximilian Demnitz,[1] Stefan Schymura,[1] F. Jankovský,[2] V. Havlová,[2] and Moritz Schmidt[1,*]

[1] Helmholtz-Zentrum Dresden – Rossendorf, Institute of Resource Ecology, Bautzner Landstr. 400, 01328 Dresden, Germany.

[2] ÚJV Řež, a.s., Hlavní 130, Řež, 250 68 Husinec, Czech Republic

[*] Corresponding author: mail: moritz.schmidt@hzdr.de; phone: +49 351 260 3156

Abstract

The interaction of Eu(III) with thin sections of migmatised gneiss from the Bukov Underground Research Facility (URF), CZ was characterized by microfocus time-resolved laser-induced luminescence spectroscopy (µTRLFS) with a spatial resolution of ~20 µm, well below typical grain sizes of the material. By this approach, sorption processes can be characterized on the molecular level while maintaining the relationship of the speciation with mineralogy and topography. The sample mineralogy was characterized by powder X-ray diffraction and Raman microscopy and the sorption was independently quantified by autoradiography using ^{152}Eu. Representative µTRLFS studies over large areas of multiple mm^2 reveal that sorption on the heterogeneous material is not dominated by any of the typical major constituent minerals (quartz, feldspar, and mica). Instead, minor phases such as chlorite and prehnite control the Eu(III) distribution, despite their low contribution to the overall composition of the material, as well as common but less studied phases like Mg-hornblende. Especially prehnite shows high a sorption uptake as well as strong binding of Eu to the mineral surface. Sorption on prehnite and hornblende happens at the expense of feldspar, which showed the highest sorption uptake in a previous spatially-resolved study on granitic rock. Similarly, sorption on quartz is reduced, even though only low quantities of strongly bound Eu(III) were found here previously. Our results illustrate how competition of mineral surfaces for adsorbing cations drives metal distribution in heterogeneous systems.

1. Introduction

The safe disposal of highly radioactive nuclear wastes – mainly spent nuclear fuel from commercial energy production, but also waste streams from nuclear fuel reprocessing and military applications – is a worldwide challenge. In the case of water intrusion into a deep geological disposal facility, interactions with the solid phases of the surrounding barrier system will control the migration of the nuclear waste components into the biosphere by being responsible for the major retention mechanisms.[1] Consequently, a sound understanding of these interactions of relevant radionuclides and mineral phases on the molecular level is a prerequisite for any safety assessment to allow reliable prediction over 100,000s of years.

Among the constituents of nuclear waste, plutonium and the minor actinides (Np, Am, and Cm) are of particular safety concern, due to their very high radiotoxicity over long periods of time. Especially ^{241}Am and ^{243}Am ($t_{1/2}$ = 432 a and 7,370 a, respectively) and ^{239}Pu ($t_{1/2}$ = 24,110 a), dominate the radiotoxicity of spent nuclear fuel over hundreds of thousands of years.[2] Americium behaves mostly lanthanide-like in solution and is essentially always trivalent under environmental conditions in aqueous solutions, but also Pu is expected to occur in its 3+ oxidation state under the strongly reducing, oxygen free conditions of a nuclear waste repository in a deep geological formation.[1,3,4] Here, we use Eu(III) as an analogue for these elements to make use of its outstanding luminescence properties[5] for microfocus time-resolved

laser-induced luminescence spectroscopy (μTRLFS).[6] Europium(III)'s ionic radius is nearly identical to its direct homologue Am(III) as well as Pu(III) [$r_{ion}^{VI}(Eu^{3+})$ = 94.7 pm, (Am^{3+}) = 97.5 pm, (Pu^{3+}) = 100.0 pm][7] and their chemical behavior is generally comparable,[8] also with respect to their interaction with mineral phases.[9,10]

Crystalline rock is a possible host rock formation for nuclear waste repositories. Some countries have already decided to construct their disposal facility for highly-radioactive nuclear waste in granite,[11,12] while others are considering crystalline rock in general as a preferred option.[13–17] Consequently, many studies have addressed the retention of relevant radionuclides on granite[6,18–21] and its components.[22–30] Such studies are complicated by the inherent heterogeneity of the material. They will contain at least the three most common main components (quartz, feldspar, and mica) to varying degrees, and a plethora of additional minor mineral phases. For single component studies to be used in safety assessment, it has to be assumed that all effects observed for the single components are additive, which overlooks competition between the materials as well as structural aspects, such as grain boundaries and surface topography. Studies addressing the heterogeneous system as a whole, on the other hand, are often purely quantitative, while mechanistic studies are rarely capable of clearly assigning molecular sorption mechanisms to a specific mineral component of the heterogeneous system.

Single component studies of the sorption of trivalent actinides, lanthanides, or rare earth elements are available for quartz,[23–25] feldspars,[22,27,30,31] and micas,[26,28,29] as well as several of the minor phases, e.g. apatite.[32–34] On both, quartz and feldspar, sorption occurs first as a bidentate inner-sphere sorption complexes around mildly acidic pH values, which are then gradually hydrolyzed at higher pH. The initial sorption step occurs at pH ~4.5 and hydrolysis begins after pH ~6.0, around pH = 7.5 complete retention is observed on both minerals. Some feldspar studies report slight variations in the pH edge[27] or speciation[30] depending on the type of cation in the Na/K/Ca-feldspar. On quartz, additionally, the formation of ternary surface complexes with silicate released by the mineral has been reported in the alkaline pH range (pH > 9.0).[24] A similar process may also occur on K-feldspar at yet higher pH (> 10).[30] Micas show different behavior depending on their composition. Biotite exhibits strongly ionic strength dependent ion exchange in its interlayer as the main interaction mechanism with trivalent metal cations, which begins at acidic pH ~ 2.5 and reaches its maximum already at pH ~ 3.5.[20] There is no structural characterization of the sorption complexes to unambiguously distinguish inner- and outer-sphere complexes, but the pH and ionic strength dependency suggests mainly outer-sphere sorption. In contrast, interaction with muscovite is *via* external surfaces instead of the interlayer.[29] Sorption also begins at acidic pH ~ 3.0, and is initially mainly outer-sphere sorption as well as extended outer-sphere sorption.[26,28] Sorption increases over a much wider pH range and becomes mostly independent of ionic strength at pH > 7.0, indicating a transition to an inner-sphere sorption mode.[28] It can be shown that the formation of inner-sphere complexes begins at pH ~ 5.0; for Y^{3+} it was shown that at pH 5.5 three

species, inner-, outer-, and extended outer-sphere sorption complex co-exist on the muscovite (001) basal plane.[26]

These studies on model systems containing only one mineral phase are essential to understand the interaction with these minerals at a high level of detail, but they cannot accurately describe the behavior of the system as a whole. For instance, studying separate mineral phases cannot reveal how sorption of Eu^{3+} on one mineral affects its sorption on the other phases, or what effect surface features such as grain boundaries, crystallite orientation, and topography have on the sorption process.[18,19,35,36] Here, studies of the whole system are required, ideally with spatial resolution to avoid the loss of connection between mineral phase and speciation described above. Several microscopic studies using a variety of techniques are available in the literature. Many studies focus on the quantitative distribution of radionuclides and their analogues,[21] often resorting to co-location with other elements to derive additional information.[20,37,38] For example, Eu^{3+} sorption on granite was studied by electron probe micro analysis (EPMA) and laser-ablation ICP-MS (LA-ICP-MS)[20,21] at low to neutral pH. Both studies show a heterogeneous distribution, mostly on biotite, which is affected by its topography and surface alteration during the sorption process. The dominance of sorption on biotite was expected based on the pH of the experiments and the sorption behavior on the pure phase. However, additional observations could not have been obtained in such studies, such as an accumulation of the metal ions at grain boundaries between quartz and feldspar.[20] A drawback of both techniques, EPMA and LA-ICP-MS is, that no information regarding the speciation at the interface can be obtained, which would be required to extrapolate the sorption behavior to other environmental conditions than the ones chosen for these studies.

More recently, spatially-resolved studies of the speciation of Eu^{3+} on granitic rocks as a whole system have become available. Ishida et al. applied luminescence imaging and combined it with Eu^{3+} luminescence lifetime measurements to obtain chemical information [time-resolved laser-induced luminescence microscopy (TRLFM)].[39] The assignment of species was then achieved by fingerprinting the decay profiles with previously measured single component data. The study finds heterogeneous sorption distributions on all components of the studied granite, which exhibit a wide range of lifetimes, except on biotite, where only the aquo ion was found. A drawback of the imaging approach is the lack of actual spectral information. While luminescence lifetimes bear information on the hydration state of Eu^{3+}, its luminescence spectra can be used to directly reveal speciation information based on the intensity ratio of the two main transitions in the spectra, ($^5D_0 \rightarrow {}^7F_1$) and ($^5D_0 \rightarrow {}^7F_2$). The former is a magnetic dipole transition, barely affected by chemical changes around the luminescing ion, while the latter is a "hypersensitive" electric dipole transition, which will strongly increase in intensity when Eu^{3+}'s ligand field changes.[5] Generally, larger band ratios ($^5D_0 \rightarrow {}^7F_2$)/($^5D_0 \rightarrow {}^7F_1$) (in the following F_2/F_1 for short) point to stronger binding to Eu^{3+}.[5] This is exploited for µTRLFS: instead of imaging luminescence intensity of a large area, the sample is scanned through the focal point of a laser beam and the whole

luminescence spectrum is recorded in each point and supplemented with lifetime measurements in select points. This process is significantly slower than TRLFM but allows unambiguously distinguishing between strongly bound species at the interface and those more weakly associated. Using this approach, we recently showed, that all main components of a granite rock from Eibenstock, Germany interact heterogeneously with Eu^{3+}.[6] This means that the Eu^{3+} distribution and speciation varies, both from mineral grain to mineral grain and within a single mineral grain. Interestingly, sorption was significantly higher on feldspar than on quartz, while the sorption strength was reversed as evidenced by very high F_2/F_1 ratios on quartz. The study also found deviating behavior at several grain boundaries, which showed increased sorption at reduced bond strength compared to the adjoining mineral grains.

Here, we present an investigation of the sorption of Eu(III) on a much more complex migmatised gneiss from the Bukov underground research facility, Czech Republic. The formation is being investigated for its suitability as a host rock for a future repository for Czech nuclear wastes,[15] and related formations on the German side of the border are equally under investigation.[40] As such, it is of utmost importance to characterize its retention properties under as realistic conditions as possible, while still obtaining molecular scale information. A thin section of the material was prepared, and characterized regarding its mineralogy by Raman microscopy and subsequently sorption and speciation of Eu(III) were characterized with 20 µm spatial resolution by µTRLFS. The results are verified by an independent sorption quantification (although with slightly lower spatial resolution), using autoradiography. We aim to identify the mineral components responsible for the retention of Eu(III) in this rock and to characterize the sorption mechanisms on the molecular level to assess the effectiveness of this retention. By comparison with the previous results on Eibenstock granite, we also aim to reveal the impact of mineral-mineral competition on the quantity and speciation of adsorbed cations.

2. Materials and Methods

2.1 Sample preparation

A drill core was obtained from the Underground Research Facility Bukov (Bukov URF), which is built in 600 m depth of a rock formation at the south end of the Rožná uranium deposit in Czech Republic, close to Brno. The geology of the site is further described in the SI, Page S1. The laboratory is used to test the suitability of this rock formation as a repository for high-level nuclear waste. A piece of this drill core was used to produce thin-sections with (20×20) mm x 150 µm in size, which are glued onto microscopy slides and finally polished. Polishing (Logitech polisher) was performed with a suspension of diamonds 1 µm and 3 µm in diameter, respectively, in ethanediol. The sample was washed with ethanol and deionized water (MilliQ, 18.2 MΩ), before the reaction with the Eu^{3+} solution.

For the µTRLFS and autoradiography measurements the thin-section was brought into contact with a Eu^{3+} solution containing the radioactive isotope ^{152}Eu (15 ml of 5×10^{-5} M [^{152}Eu]Eu^{3+} (A ≈ 17 kBq) with

0.1 M NaCl background electrolyte). The pH was adjusted to 7.5 by adding NaOH and HCl. That pH was chosen, because sorption reaches its maximum in the pH edge experiments, while homogeneous precipitation of Eu solids is still very low. These findings are based on batch sorption experiments, which are described in more detail in the SI, Page S1 and Figure S1. To conduct the sorption experiment, the sample was put upside down in a watch glass to avoid any sorption on the backside of the sample, which would lead to interfering signals in the autoradiography measurement. The watch glass was filled with the europium solution, so that the liquid surface was covering the whole sample on the mineral side for 5 days. Liquid levels were readjusted on a daily basis. After the sorption experiment the sample was washed gently with MilliQ water (18.2 MΩ) to avoid precipitation.

2.2 Powder X-ray Diffraction

Different parts of the drill core were thoroughly pulverized using a McCrone mill. The powder X-ray diffraction data was collected on a Bruker D8 Advance powder diffractometer in a Bragg-Brentano geometry. CuKα radiation and Lynx Eye XE detector were used. The data was collected in the angular range 4-80° of 2Θ with a 0.015° step and 0.8 sec time per step. The qualitative phase analysis was performed using the Diffrac.Eva 4.1 program (Bruker AXS, Germany, 2015) with the help of the PDF-2 database. Subsequently, the semi quantitative phase analysis was performed by the Rietveld method[41] using the Topas 5 (Bruker AXS, Germany, 2014) software suite. The results of both analyses are shown in the SI, Figure S2 and S3. The crystal structures of mineral phases used in the refinement were obtained from the ICSD database (FIZ Karlsruhe, Germany, 2018). During the Rietveld refinement, only the scale factors, unit-cell parameters, and size of coherent-diffracting domains were refined. A correction for preferred orientation was applied for selected mineral phases (e.g. biotite, K-feldspar, labradorite). Limits of detection vary in the range 0.2-0.5 wt%.

2.3 Raman microscopy

Before sorption experiments were conducted, Raman mappings of the mineralogy were determined for the unloaded thin section and a (3×4) mm^2 ROI was chosen based on the presence of many visually different features (used as an indicator for different mineral phases). A grid of (20×20) μm^2 was used resulting in around 26000 single Raman spectra. These spectra were evaluated with a Python-based software (pycroTRLFS EVAL, HZDR, Germany) regarding their peak positions and compared to spectra from the RRUFF database to identify the mineral phases.[42] Representative measured spectra compared to reference spectra are available in the SI, Figure S4. Spectra were measured with a LabRAM ARAMIS (Horiba, Japan) Raman microscope combined with a 532 nm cw-laser (50 mW). Slit and pin-hole diameter were set to 200 µm. Spectral resolution was set by a 600 lines/mm grating.

2.4 µTRLFS

µTRLFS measurements were performed with a specially designed setup, which was already described in our previous work.[6] Briefly, A laser beam (Surelite SL I-20 @355 nm pump laser, Continuum with NarrowScanK @Exalite 389/398 mix dye laser, Radiant Dyes) was coupled into the setup by a dichroic mirror (490 nm cut-off wavelength, Thorlabs). The redirected beam was then focused onto the sample by an objective (HCX APO 10×, Leica). The sample was placed on an XYZ motorized stage (Newport). The emitted luminescence is collected and collimated by the focusing objective, passes the dichroic mirror and is focused by a second lens (achromatic, f = 100 mm, Thorlabs) onto the tip of a light guide. The light guide was connected to a spectrometer (Shamrock SR303i spectrograph with DH320T-18U-63 iCCD camera, Andor, UK) for detection. A lower laser pulse energy of around 20 µJ was used to avoid laser ablation on the sample. A 300 l/mm grating was used in the polychromator and a delay of 1 µs after the laser pulse with a gate width of 10 ms was chosen, to protect the detector from laser light and collect the entire luminescence emission, respectively. In total around 6700 single luminescence spectra were recorded in the three chosen µTRLFS ROIs.

The luminescence of the two main emission transitions of Eu^{3+} ($^5D_0 \rightarrow {}^7F_1$) and ($^5D_0 \rightarrow {}^7F_2$) was evaluated by a Python-based software (pycroTRLFS EVAL, HZDR, Germany) by first applying a linear background correction for each peak and then integrating both peaks separately spectrum by spectrum. The sum of intensities (F_1+F_2) and the intensity ratio (F_2/F_1) were then assigned to the coordinates of the spectra, which results in a mapping of the sorption uptake (total luminescence intensity, F_1+F_2) and speciation or sorption strength respectively (peak ratio, F_2/F_1). It should be noted here that comparisons of the luminescence intensity are contingent on the absence of quench processes, as could be induced by e.g. iron. In the minerals with a high Fe content (see below) this will effectively lead to complete extinction of the luminescence signal, but other parts of the sample may also be affected. Typically, the presence of quenchers in addition to water can be derived from the detection of lifetimes shorter than the aquo ion's lifetime (see below), but lifetimes measurements are only available in select points.

Lifetime analysis of the luminescence decay was done point by point at selected pixels. For this, spectra were measured with varying time delays relative to the laser pulse, got background corrected and the total luminescence intensity was approximated by mono-, bi- or tri-exponential decay curves depending on convergence and residuals to obtain the lifetime values. The lifetimes were then used to calculate the corresponding number of water molecules remaining in the first coordination sphere of Eu^{3+} with the following empirical equation.[43–45]

$$n(H_2O) \pm 0.5 = \frac{1.07\ \text{ms}}{\tau[\text{ms}]} - 0.62 \qquad \text{Eq. 1}$$

The Eu^{3+} aquo ion has nine water molecules in its hydration sphere.[45–47] When measuring surface-bound species, a coordination number of nine indicates an outer-sphere (OS) sorption species with no loss of the hydration sphere. A lower number of water molecules indicates inner-sphere (IS) sorption, with a partial loss of the hydration sphere and a direct bond between Eu^{3+} and the surface. Low values

of n = 1-3 can be interpreted as a surface (SF) incorporation species with Eu^{3+} partially imbedded into the mineral surface.[32,48,49] A total loss of hydration indicates full incorporation into the mineral, which likely stems from intrinsic Eu^{3+} impurities of the natural material, due to the short duration of our experiments.

2.5 Autoradiography

To conduct the autoradiography measurements the loaded sample was placed on a BAS-IP MS image plate (GE Lifesciences) and put into a light-tight aluminum cassette to press both on top of each other, separated by a plastic wrap to avoid contamination. After exposure of the image plate at different positions over several time frames, it was read out using an Amersham Typhoon Biomolecular Imager (GE Lifesciences) with a pixel size of 10 µm. The data of the 120 min exposure time was chosen for further analysis due to the highest dynamic range. The actual resolution is expected to be lower than the 10 µm read-out. One reason is the isotropic radiation combined with the distance between sample and image plate due to the plastic wrap. Scattering by the foil and the backscattering from the surface will additionally lower the effective resolution.

3. Results

3.1 Mineralogy

The PXRD measurements show, that the Bukov sample is mainly composed of feldspar, amphibole, quartz and mica (feldspar: 44.8 wt% plagioclase, 0.7 wt% alkali-feldspar; amphibole: 30.3 wt% Mg-hornblende; quartz: 13.5 wt%; and mica: 9.2 wt% biotite and 1.5 wt% chlorite, on average over three fractions of the sample). Based on a former study, the Bukov rock is classified as migmatised amphibole-biotitic paragneiss to migmatised biotitic paragneiss with amphibole.[50] The Bukov rock is characterized by a distinctive mineralogical heterogeneity and spatial variability. For simplicity, we will refer to the material as migmatised gneiss in the following. A detailed qualitative analysis of the PXRD spectra shows additional minor minerals like prehnite, apatite and kaersutite as another member of the amphibole mineral group. This macroscopic mineralogy just serves as a starting point for the mineral phase identification with Raman microscopy of a region of interest (ROI) on a thin-section of the Bukov migmatised gneiss.

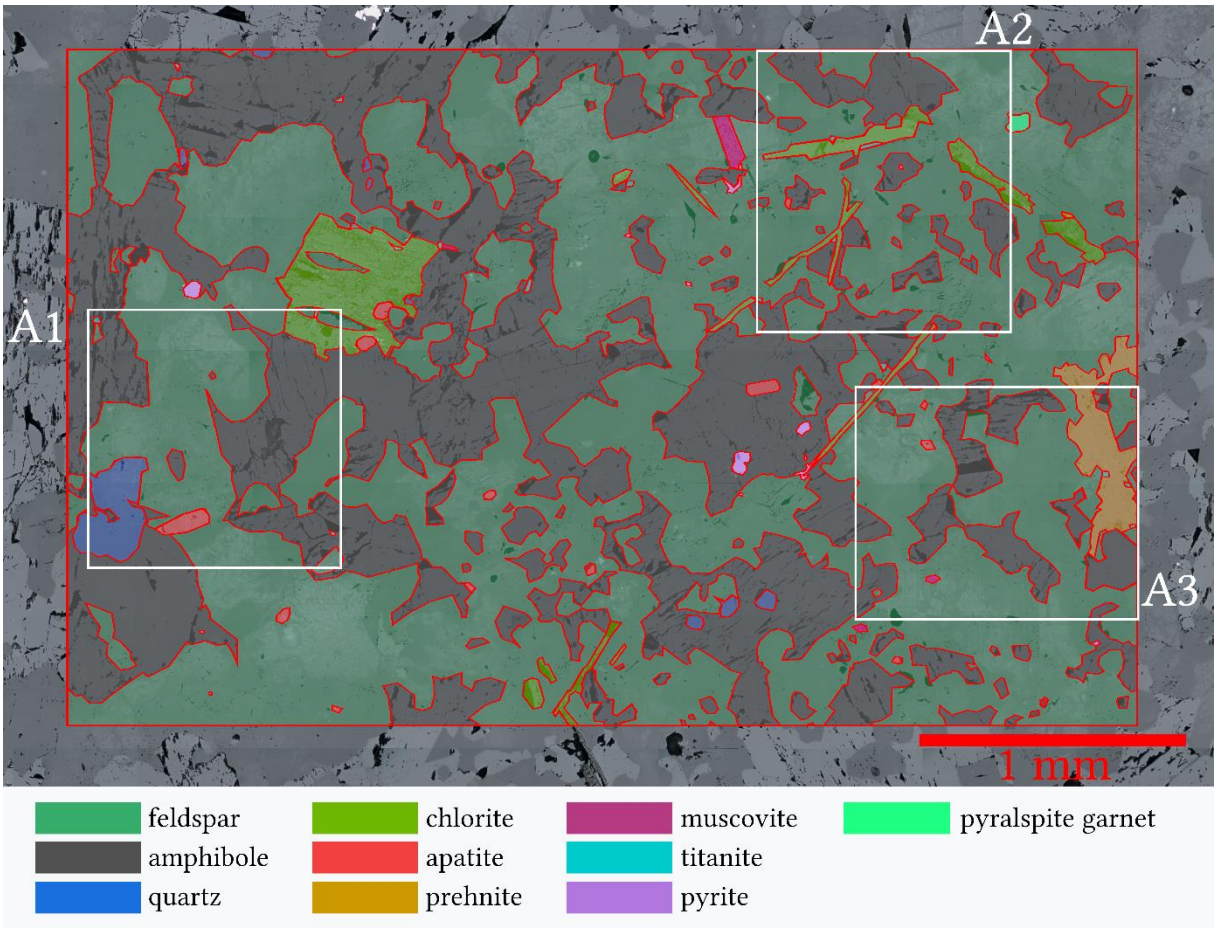

Figure 1: Raman-based mineralogy and µTRLFS-ROIs (white rect.) with feldspar, amphibole, quartz, chlorite, apatite, prehnite, muscovite, titanite, pyrite, and pyralspite garnet mineral grains separated by red grain boundaries.

In Figure 1 the Raman-based mineralogy of the ROI is shown along with µTRLFS-ROIs A1 to A3 marked in white. As expected, most of the ROI is covered with the main minerals already identified by PXRD. Additionally, titanite, pyrite, and pyralspite garnet could be identified. Mineral grains identified as chlorite could also be a mix of biotite and chlorite, as the Raman spectra are not definitive, but the needle-like morphology is more common for chlorite.[51,52] As most of these secondary minerals are not identified by the quantitative PXRD analysis, the total amount should be low on average. Within the area marked in red in Figure 1, the mineral composition by area is 58.1 % feldspar, 36.4 % amphibole, 3.0 % chlorite, 1.0 % prehnite, 0.9 % quartz, 0.3 % apatite, 0.2 % muscovite, 0.1 % pyrite, 0.1 % titanite and 0.1 % pyralspite garnet. Titanite forms only tiny mineral grains, which are hardly visible in the mineralogy; the spectral identification is nonetheless reliable.

3.2 µTRLFS: Local Eu^{3+} speciation and sorption uptake

To investigate the sorption behavior of Eu^{3+}, in contact with Bukov migmatised gneiss, three ROIs, which contain most of the identified minerals, were measured with µTRLFS and evaluated regarding the sorption uptake and speciation as already explained in the methods section. In the following

µTRLFS-ROI A3 mappings will be presented in detail, while A1 and A2 mappings and all lifetimes can be found in the SI, Figure S5, S6 and S7. The following discussion will take all ROIs into account.

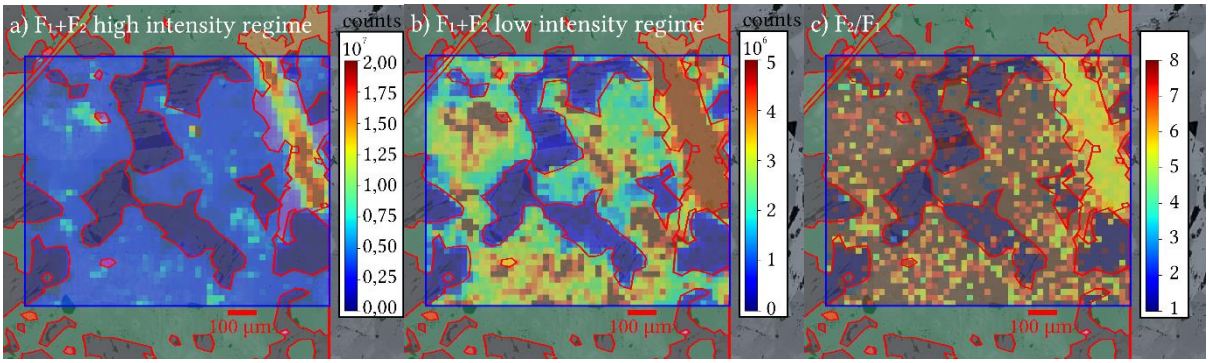

Figure 2: µTRLFS mappings of ROI A3 of sorption uptake (F_1+F_2) in the high (a) and low intensity regime (b) and speciation (F_2/F_1) (c) with highlighted grain boundaries in red

In Figure 2 the µTRLFS mappings of ROI A3 are visualized. The sorption uptake is shown with two different intensity regimes, so that the differences in areas with a low luminescence intensity can be identified better. For all of the ROIS the luminescence intensity distribution is mostly correlated with the crystal grains and the intensities between different mineral grains can vary from lowest to highest by a factor of 100. Additionally, to this inter-grain variation of the sorption uptake also distinct intra-grain variations can be observed, especially on feldspar, with intensities varying by a factor of 10. Prehnite, which is located on the upper right of the mapping (cp. Figure 1), has the highest observed luminescence intensities within all ROIs. Apatite (A1, A3) has a nearly as high sorption uptake as Prehnite. On amphibole grains, the luminescence intensity is very low, but a Eu^{3+} signal is still detectable, while grain boundaries to feldspar partially show a higher sorption uptake (A1). The same grain boundary effect can also be observed in the case of the quartz mineral grain (A1). On pyrite, titanite and chlorite there is no Eu^{3+} luminescence detectable, due to the high Fe content in these minerals quenching Eu^{3+} luminescence.

In Figure 2 c) the speciation mapping of ROI A3 is shown as a distribution of luminescence peak ratios, F_2/F_1. Prehnite not only has the highest sorption uptake, but also the highest evaluable peak ratio of 5 to 6 within all ROIs, which is homogeneously distributed over the whole grain. This indicates strong binding over the whole mineral grain surface. On feldspar we typically find slightly lower peak ratios of 4 to 5, where luminescence intensity is high. In the areas of low overall intensity, the F_1 peak becomes indistinguishable from the background, which precludes a numerical analysis. The F_2 band is still prominent in these areas, which suggests fairly high band ratios. The peak ratios on apatite are also hard to quantify. In this case the F_1 band overlaps with luminescence of non-Eu^{3+} fluorophores. The spectral fingerprint of Eu^{3+} is still evident, but an evaluation of the band ratio becomes impossible. Representative spectra of feldspar hot spots and bulk, prehnite and apatite are shown in the SI, Figure S8. Minerals with a very low luminescence intensity like quartz, amphibole, or chlorite cannot be

evaluated regarding their peak ratio. Here it is noteworthy that in our previous study[6], luminescence intensity on quartz was also relatively low but still well sufficient for a band ratio analysis.

Table 1: Species identified on each mineral based on lifetime analysis and the number of corresponding water molecules in Eu^{3+}'s first coordination sphere. Uncertainties represent distribution of values determined on multiple spots wherever possible.

Mineral	***n* (H_2O)**	***Species***
Apatite	*0.4 ± 0.5*	*Intrinsic incorporation*
	2.8 ± 0.9	IS sorption
Feldspar	3.1 ± 0.5	SF incorporation (common)
	5.1 ± 0.5	IS sorption (interm.)
	7.3 ± 0.5	IS sorption (rare)
	0.2 ± 0.3	*Intrinsic incorporation*
Prehnite	5.8 ± 1.0	IS sorption
	2.5 ± 0.8	SF incorporation
	9.0 ± 0.9	OS sorption
	0.2 ± 0.2	*Intrinsic incorporation*
Pyralspite garnet	1.4 ± 0.3	SF incorporation
	0.0 ± 0.1	*Intrinsic incorporation*
Quartz*	0.4 ± 0.4	*Intrinsic incorporation (likely into feldspar)*

In Table 1 all identified species based on a total of 44 lifetime measurements are listed (see SI, Figure S7 and Table S1 for locations and determined lifetimes). Omitted mineral phases showed too low luminescence intensity for reliable lifetime analysis. Taking the F_2/F_1 band ratios into account, we can use the number of water molecules remaining in the first coordination sphere of Eu^{3+} to identify the type of sorption complexes formed on each mineral. On feldspar we find a total of four different species, a surface incorporation species, two inner-sphere sorption complexes differing in their degree of hydration, and an incorporation species. The latter must be Eu^{3+} intrinsically present in the mineral, as an incorporation process seems unlikely in the short duration of our experiments. This is corroborated by the observation that this species is present over the whole surface of the mineral and appears most prominently where the total luminescence intensity is low. The inner-sphere sorption species show a wide distribution of hydration with 3, 5, or 7 water molecules remaining in the hydration spheres, respectively. The species with only three remaining water molecules is by far the most common, accounting for more than 70% of the inner-sphere complexes, while around 20% exhibit five water molecules and only ~7% maintain the highest number of water molecules. In our previous study,[6] the

same incorporation species was also identified, as well as the IS complex with seven remaining water molecules. However, on K-feldspar in Eibenstock granite, this IS complex was dominating the Eu^{3+} speciation and any other IS complex was too minor to be identified. The grain boundaries between feldspar and amphibole, which showed increased sorption of Eu^{3+} relative to bulk amphibole, also reveal a feldspar-like speciation, confirming that here amphibole is likely covered by a thin layer of feldspar.

On prehnite we can also identify four different species, three sorption complexes and Eu^{3+} intrinsically incorporated into the mineral. Sorption occurs as both, IS sorption characterized by lifetimes corresponding to hydration by about six water molecules and as a surface incorporation species[9] with shorter lifetimes corresponding to 1.5 to 3.5 coordinating water molecules. Both modes of surface bonding appear with similar frequency, which explains the homogeneous distribution of band ratios on prehnite (Figure 2c). Close to the mineral grain boundaries, also very short lifetimes, which belong to the Eu^{3+} aquo ion were determined, albeit with relatively large uncertainties. This would indicate an outer-sphere sorption mechanism for these areas.

Two lifetimes can be determined on apatite, corresponding to complete loss of hydration and coordination by three water molecules, respectively. Here again, interpretation of the data is complicated by overlap with luminescence unrelated to Eu^{3+}. This impurity luminescence has a very similar lifetime as the long-lived Eu^{3+} species, which leads to a large uncertainty in the determination of this lifetime. As discussed for incorporation into feldspar, we assume most incorporation to be unrelated to our experiments, but rather intrinsic Eu^{3+} (representative spectra are shown in the SI, Figure S9). However, incorporation of Eu^{3+} into apatite has been shown to occur rapidly under some conditions (see below).[32] The second species can be interpreted as a surface (SF) incorporation species, due to its relatively low number of bound water molecules.

On quartz lifetime determination was only possible close to the grain boundary with feldspar, where the luminescence intensity was slightly higher. The species we identify here is a fully dehydrated incorporation species, with a spectral fingerprint matching that of the incorporation species in feldspar, once again confirming that these grain boundaries exhibit layering of two minerals. Therefore, these lifetimes cannot be considered typical of the speciation of Eu^{3+} on quartz grains in Bukov migmatised gneiss. On pyralspite we once again find only surface incorporation and intrinsic incorporation into the bulk of the mineral.

3.3 Autoradiography: Eu^{3+} sorption uptake comparison

Autoradiography allows us to independently quantify the sorption of Eu^{3+} on the migmatised gneiss surface. The method is not affected by luminescence quenching by transition metals and hence all minerals can be considered and the use of radioactive ^{152}Eu ensures that only Eu from our sorption experiments is detected (as opposed to intrinsically incorporated Eu). The autoradiogram (Figure 3) was

recorded for the same ROI that was used for the mineral identification with a nominally similar resolution (~10 µm) as µTRLFS. Due to the specific conditions of the measurement, the actual resolution is however significantly lower (~100 µm).

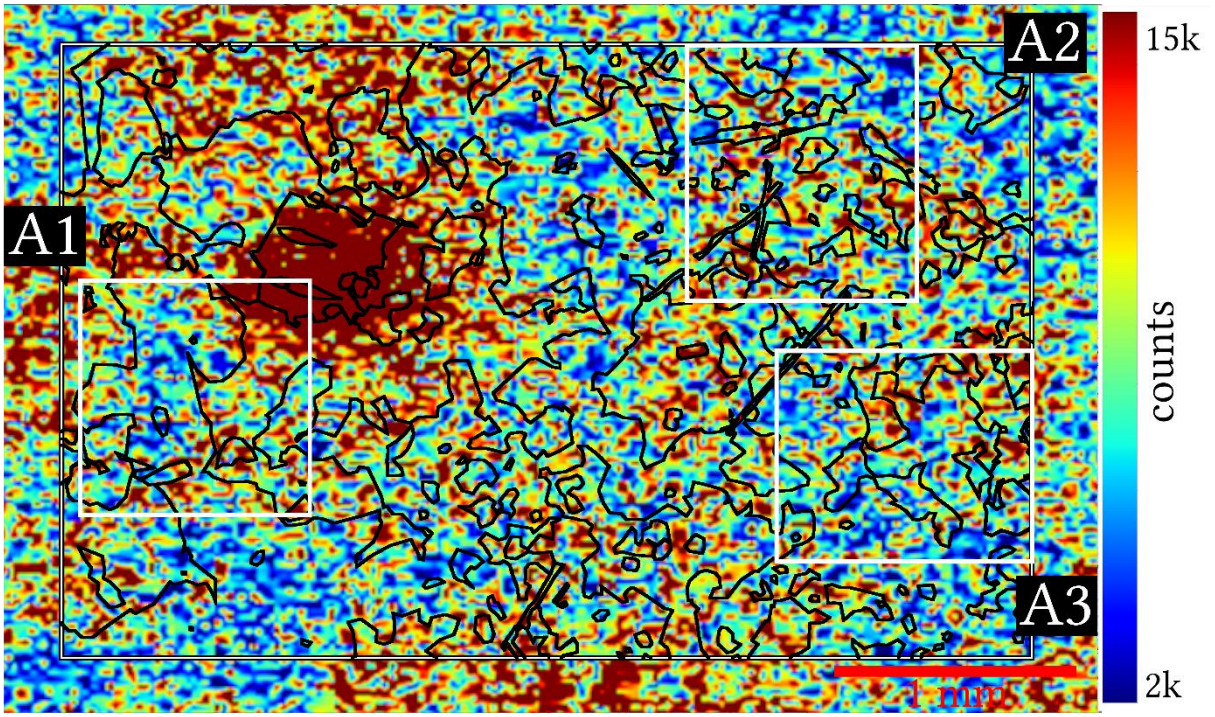

Figure 3: Autoradiogram of the same ROI as used in Figure 1 with highlighted µTRLFS ROIs (white rectangles)

Radiographically, the chlorite grain on the upper left (cp. Figure 1) exhibits the highest Eu^{3+} deposition in the whole ROI. Other chlorite grains also show high sorption uptake, but not as prominent as the largest grain. Sorption is somewhat lower on amphibole and prehnite, which exhibit very similar sorption capacities. Sorption on feldspar is significantly lower than on the previously mentioned minerals. There is no observable difference between feldspar, quartz, and apatite. All the other minerals, which only occur as very small grains cannot be reliably evaluated due to the low resolution of the method. As the autoradiogram is noisy, especially in those regions with a lower sorption uptake, an absolute quantification of the Eu^{3+} was not feasible, but a relative sorption uptake can be determined: chlorite > amphibole ≈ prehnite > feldspar ≈ quartz ≈ apatite.

The sequence of mineral reference agrees with the µTRLFS findings, with the notable exceptions of chlorite and amphibole, which are not accessible to µTRLFS measurements due to their high Fe contents. As mentioned in the experimental section, other discrepancies may arise from the significantly lower resolution of the autoradiography measurement due to the isotropic radiation and scattering by the plastic wrap and the surface itself.

3.2 Discussion

The sorption behavior of Eu^{3+} on Bukov migmatised gneiss can be briefly summarized as follows. Quantitatively, the overall sorption uptake is controlled by chlorite, amphibole, and prehnite, with only low sorption on feldspar and quartz. We can only obtain speciation information where µTRLFS is not affected by quenching by e.g. iron or very low luminescence intensities. Here, we find relatively strong inner-sphere complexes on feldspar, but also on prehnite, where additional surface incorporation was observed. On quartz, no characterization was possible due to the very low Eu^{3+} sorption on its surface. Sorption on apatite appears to be quite high, but an interpretation is complicated by additional luminophores in the natural material. Nevertheless, the species can be tentatively identified as a surface incorporation species and fully incorporated Eu^{3+}. The incorporated Eu^{3+} is most likely intrinsic[53] and not a consequence of the sorption experiment, although some studies suggest rapid incorporation into apatite is possible.[32]

These findings illustrate the complexity of sorption processes on natural materials and particularly shed light on the effect of mineral competition on sorption processes, as becomes clear when comparing the distribution of Eu^{3+} on Bukov migmatised gneiss to the previously determined distribution on Eibenstock granite.[6] The previously investigated system had a significantly simpler composition of only K-feldspar, quartz, and biotite. It quickly becomes clear that the mineral phases that dominate retention of Eu on Bukov migmatised gneiss were not present in Eibenstock granite, which affects the interaction with the mineral phases present in both rocks.

This is most obvious for feldspar, where the competition affects the quantity of adsorbed Eu^{3+}, which in turn affects its speciation. In the previous study on Eibenstock granite, feldspar was the main surface for metal retention especially at high pH. Here, on the other hand, feldspar exhibits low to medium Eu^{3+} sorption and is clearly outcompeted by other phases, according to both autoradiography and µTRLFS. At the same time, sorption to feldspar has become stronger, as evidenced by the lower number of water molecules (and hence larger number of surface coordinating groups) in Eu's first coordination sphere. On Eibenstock granite feldspar, typically ~7 water molecules remain with adsorbed Eu^{3+}, corresponding to mono- or bidentate binding to the surface. While we find the same species on feldspar in Bukov migmatised gneiss, the larger fraction of adsorbed Eu^{3+} is coordinated by 3 or 5 water molecules, which indicates a higher coordination number from the surface. In addition, surface incorporation with only 1-2 remaining water molecules is observed. Apparently, binding to feldspar in Bukov migmatised gneiss only occurs at preferential sites offering strong binding by multiple surface groups, which presumably, goes along with a low reversibility of the sorption process. As sorption on feldspar in Bukov gneiss is low, the weaker sorption sites, which dominated sorption on feldspar in Eibenstock granite, are rarely occupied. Thus, the weakly bound IS complex identified on Eibenstock granite is almost completely replaced by sorption on more preferable mineral phases like prehnite or chlorite. A similar effect though with lower sorption uptake overall can be seen on quartz, where sorption was low, but the sorption interaction was fairly strong on Eibenstock granite. This was interpreted as a preferential occupation of

defect sites, which can bind through multiple surface sites. Through the competition with prehnite, chlorite, and hornblende, sorption on quartz is nearly completely suppressed in this study, to such an extent that a characterization of Eu^{3+}'s speciation on quartz was no longer possible.

The observed changes in speciation appear to lead to the preferred occupation of sorption sites with very low number of water molecules remaining with Eu^{3+}, strong IS complexes or even surface incorporation species. It seems reasonable to assume that the formation of such species will require surface defects, as an atomically flat mineral surface without kinks or steps would not be able to provide six or even eight binding groups. As the spatial resolution of our experiments is, however, significantly larger than these atomic defects, the observed speciation must be a consequence of an increased density of defects in the areas, where such strong sorption modes dominate. This connection between surface topography and sorption preference and speciation should be investigated in more detail.

3.3 Environmental Implications

This study proves once more the importance of sorption studies on whole natural rock samples at the molecular level. The interaction with mineral phases controls the mobility of contaminants and radionuclides at contaminated sites and technical installations, such as a deep geological repository for nuclear waste. Safety assessment and remediation strategies for such sites frequently rely on reactive transport modelling based on thermodynamic constants derived from sorption studies. As our results demonstrate, the speciation and sorption uptake will depend on the combination of mineral phases present and sorption on one phase may significantly change the amount of adsorbed Eu^{3+} on another. Where multiple types of binding sites exist, this competition will also affect the speciation of the adsorbed cation. This type of behavior cannot be studied in single phase systems but must be investigated in systems as close to reality as possible. Single phase model studies will of course remain important as the foundation necessary for the understanding of more complex systems.

One such system was here identified in prehnite, which may be a highly relevant mineral phase for the retention of trivalent actinides, such as Am^{3+} from nuclear wastes, in repositories located in crystalline rock. It is known to be a fracture filling material[54–56] and will exhibit accessible surfaces in contact with a presumed water flow path through the material. Our results indicate prehnite may serve as an effective barrier for the transport of radionuclides in this scenario, but detailed and quantitative studies are to the best of our knowledge absent from the literature. The situation for the other mineral phases, which control the retention of Eu^{3+} in our study is similar; also, for chlorite and Mg-hornblende data on their retention potential is very limited, both thermodynamically and on the molecular level.

To expand the applicability of our findings to a broader range of scenarios such detailed studies on the model systems will be required. In addition, attempts must be made to accurately reproduce

spectroscopically verified distributions of Eu^{3+} on natural rock using surface complexation modelling and reactive transport calculations, which would allow to better evaluate both, the quality of current models and the relevance of our molecular scale information on the larger scale.

References

(1) Geckeis, H.; Lützenkirchen, J.; Polly, R.; Rabung, T.; Schmidt, M. Mineral–Water Interface Reactions of Actinides. *Chem. Rev.* **2013**, *113* (2), 1016–1062.

(2) Gonzalez, E. *Physics and Safety of Transmutation Systems, Status Report*; 2006.

(3) Clark, D. L.; Hecker, S. S.; Jarvinen, G. D.; Neu, M. P. Plutonium. In *The Chemistry of the Actinide and Transactinide Elements*; Morss, L. R., Edelstein, N. M., Fuger, J., Katz, J. J., Eds.; Springer, 2011; Vol. 2, pp 1265–1395.

(4) Runde, W. H.; Schulz, W. W. Americium. In *The Chemistry of the Actinide and Transactinide Elements*; Morss, L. R., Edelstein, N. M., Fuger, J., Katz, J. J., Eds.; Springer, 2011; Vol. 2, pp 813–1264.

(5) Binnemans, K. Interpretation of Europium(III) Spectra. *Coord. Chem. Rev.* **2015**, *295*, 1–45.

(6) Molodtsov, K.; Schymura, S.; Rothe, J.; Dardenne, K.; Schmidt, M. Sorption of Eu(III) on Eibenstock Granite Studied by MTRLFS: A Novel Spatially-Resolved Luminescence-Spectroscopic Technique. *Sci. Rep.* **2019**, *9* (6287), 6287.

(7) Shannon, R. D. Revised Effective Ionic Radii and Systematic Studies of Interatomie Distances in Halides and Chaleogenides. *Acta Crystallogr.* **1976**, *32*, 751–767.

(8) Silva, R. J.; Nitsche, H. Actinide Environmental Chemistry. *Radiochim. Acta* **1995**, *70/71*, 377–396.

(9) Schmidt, M.; Stumpf, T.; Fernandes, M. M.; Walther, C.; Fanghänel, T. Charge Compensation in Solid Solutions. *Angew. Chemie Int. Ed.* **2008**, *47*, 5846–5850.

(10) Schnurr, A.; Marsac, R.; Rabung, T.; Lützenkirchen, J.; Geckeis, H. Sorption of Cm(III) and Eu(III) onto Clay Minerals under Saline Conditions: Batch Adsorption, Laser-Fluorescence Spectroscopy and Modeling. *Geochim. Cosmochim. Acta* **2015**, *151* (0), 192–202.

(11) Oy, P. *Safety Case for the Disposal of Spent Nuclear Fuel at Olkiluoto, Report*; 2012.

(12) Svensk Kärnbränslehantering AB. *Long-Term Safety for the Final Repository for Spent Nuclear Fuel at Forsmark, Report*; 2011.

(13) Wang, J. High-Level Radioactive Waste Disposal in China: Update 2010. *J. Rock Mech.*

Geotech. Eng. **2010**, *2* (1), 1–11.

(14) Laverov, N. P.; Yudintsev, S. V; Kochkin, B. T.; Malkovsky, V. I. The Russian Strategy of Using Crystalline Rock as a Repository for Nuclear Waste. *Elements* **2016**, *12*, 253–256.

(15) SURAO. *Annual Report*; 2017.

(16) Mariner, P. E.; Stein, E. R.; Kalinina, E. A.; Hadgu, T.; Jove-Colon, C.; Basurto, E. *US Sections Prepared for Future NEA Crystalline Club (CRC) Report on Status of R&D in CRC Countries Investigating Deep Geologic Disposal in Crystalline Rock, Report*; 2018.

(17) Bundestag. Gesetz Zur Suche Und Auswahl Eines Standortes Für Ein Endlager Für Hochradioaktive Abfälle (Standortauswahlgesetz - StandAG). 2017.

(18) Allard, B.; Beall, G. W.; Krajewski, T. The Sorption of Actinides in Igneous Rocks. *Nucl. Technol.* **1980**, *49* (3), 474–480.

(19) Baik, M. H.; Cho, W. J.; Hahn, P. S. Effects of Speciation And Carbonate on The Sorption of Eu(3) Onto Granite. *Environ. Eng. Res.* **2004**, *9* (4), 160–167.

(20) Fukushi, K.; Hasegawa, Y.; Maeda, K.; Aoi, Y.; Tamura, A.; Arai, S.; Yamamoto, Y.; Aosai, D.; Mizuno, T. Sorption of Eu(III) on Granite: EPMA, LA–ICP–MS, Batch and Modeling Studies. *Environ. Sci. Technol.* **2013**, *47* (22), 12811–12818.

(21) Jin, Q.; Wang, G.; Ge, M.; Chen, Z.; Wu, W.; Guo, Z. The Adsorption of Eu(III) and Am(III) on Beishan Granite: XPS, EPMA, Batch and Modeling Study. *Appl. Geochemistry* **2014**, *47*, 17–24.

(22) Stumpf, S.; Stumpf, T.; Walther, C.; Bosbach, D.; Fanghaenel, T. Sorption of Cm(III) onto Different Feldspar Surfaces: A TRLFS Study. *Radiochim. Acta* **2006**, *94* (5), 243–248.

(23) Stumpf, S.; Stumpf, T.; Lützenkirchen, J.; Walther, C.; Fanghänel, T. Immobilization of Trivalent Actinides by Sorption onto Quartz and Incorporation into Siliceous Bulk: Investigations by TRLFS. *J. Colloid Interface Sci.* **2008**, *318* (1), 5–14.

(24) Takahashi, Y.; Murata, M.; Kimura, T. Interaction of Eu(III) Ion and Non-Porous Silica: Irreversible Sorption of Eu(III) on Silica and Hydrolysis of Silica Promoted by Eu(III). *J. Alloys Compd.* **2006**, *408–412*, 1246–1251.

(25) Kuta, J.; Wander, M. C. F.; Wang, Z.; Jiang, S.; Wall, N. A. Trends in Ln(III) Sorption to Quartz Assessed by Molecular Dynamics Simulations and Laser-Induced Fluorescence Studies. *J. Phys. Chem. C* **2011**, *115*, 21120–21127.

(26) Lee, S. S.; Schmidt, M.; Laanait, N.; Sturchio, N. C.; Fenter, P. Investigation of Structure,

Adsorption Free Energy, and Overcharging Behavior of Trivalent Yttrium Adsorbed at the Muscovite (001)–Water Interface. *J. Phys. Chem. C* **2013**, *117* (45), 23738–23749.

(27) Li, P.; Wu, H.; Liang, J.; Yin, Z.; Pan, D.; Fan, Q.; Xu, D.; Wu, W. Sorption of Eu(III) at Feldspar/Water Interface: Effects of PH, Organic Matter, Counter Ions, and Temperature. *Radiochim. Acta* **2017**, *105* (12), 1049–1058.

(28) Pan, D.; Fan, F.; Wang, Y.; Li, P.; Hu, P.; Fan, Q.; Wu, W. Retention of Eu(III) in Muscovite Environment: Batch and Spectroscopic Studies. *Chem. Eng. J.* **2017**, *330*, 559–565.

(29) Sasaki, G.; Niibori, Y.; Mimura, H.; Kirishima, A. Estimation of Sorption Behavior of Europium(III) Using Biotite Flakes - 13272. *WM2013 Waste Manag. Conf. Int. Collab. Contin. Improv.* **2013**, No. 13272, 13272.

(30) Neumann, J.; Brinkmann, H.; Britz, S.; Lützenkirchen, J.; Bok, F.; Stockmann, M.; Brendler, V.; Stumpf, T.; Schmidt, M. A Comprehensive Study of the Sorption Mechanism and Thermodynamics of F-Element Sorption onto K-Feldspar. *J. Colloid Interface Sci.* **2020**.

(31) Nagasawa, H. Partitioning of Eu and Sr between Coexisting Plagioclase and K-Feldspar. *Earth Planet. Sci. Lett.* **1971**, *13*, 139–144.

(32) Holliday, K.; Dardenne, K.; Walther, C.; Stumpf, T. The Incorporation of Europium into Apatite: A New Explanation. *Radiochim. Acta* **2013**, *101*, 267–272.

(33) Rakovan, J.; Reeder, R. J. Intracrystalline Rare Earth Element Distributions in Apatite: Surface Structural Influences on Incorporation during Growth. *Geochim. Cosmochim. Acta* **1996**, *60*, 4435–4445.

(34) Ohnuki, T.; Kozai, N.; Isobe, H. Sorption Mechanism of Europium by Apatite Using Rutherford Backscattering Spectroscopy. *J. Nucl. Sci. Technol.* **1997**, *34* (1), 58–62.

(35) Nebelung, C.; Brendler, V. U(VI) Sorption on Granite: Prediction and Experiments. *Radiochim. Acta* **2010**, *98*, 621–625.

(36) Holgersson, S. Studies on Batch Sorption Methodologies: Eu Sorption onto Kivetty Granite. *Procedia Chem.* **2012**, *7*, 629–640.

(37) Fröhlich, D. R.; Amayri, S.; Drebert, J.; Grolimund, D.; Huth, J.; Kaplan, U.; Krause, J.; Reich, T. Speciation of Np(V) Uptake ByOpalinus Clay Using Synchrotron Microbeam Techniques. *Anal. Bioanal. Chem.* **2012**, *404*, 2151–2162.

(38) Baik, M. H.; Hyun, S. P.; Cho, W. J.; Hahn, P. S. Contribution of Minerals to the Sorption of U(VI) on Granite. *Radiochim. Acta* **2004**, *92*, 663–669.

(39) Ishida, K.; Kimura, T.; Saito, T.; Tanaka, S. Adsorption of Eu(III) on a Heterogeneous Surface Studied by Time-Resolved Laser Fluorescence Microscopy (TRLFM). *Environ. Sci. Technol.* **2009**, *43* (6), 1744–1749.

(40) Kommission Lagerung hoch radioaktiver Abfallstoffe. *Abschlussbericht, Report*; 2016.

(41) Bish, D. L.; Post, J. E. *Reviews in Mineralogy, Review*; 1989.

(42) Lafuente, B.; Downs, R. T.; Yang, H.; Stone, N. The Power of Databases: The RRUFF Project. *Highlights Mineral. Crystallogr.* **2015**.

(43) Choppin, G. R.; Peterman, D. R. Application of Lanthanide Luminescence Spectroscopy to Solution Studies of Coordination Chemistry. *Coord. Chem. Rev.* **1998**, *174* (174), 283–299.

(44) Horrocks, W. D.; Sudnick, D. R. Lanthanide Ion Probes of Structure in Biology. Laser-Induced Luminescence Decay Constants Provide a Direct Measure of the Number of Metal-Coordinated Water Molecules. *J. Am. Chem. Soc.* **1979**, *101* (2), 334–340.

(45) Kimura, T.; Choppin, G. R. Luminescence Study on Determination of the Hydration Number of Cm(III). *J. Alloys Compd.* **1994**, *213/214*, 313–317.

(46) Barthelemy, P. P.; Choppin, G. R. Luminescence Study of Complexation of Europium and Dicarboxylic Acids. *Inorg. Chem.* **1989**, *28*, 3354–3357.

(47) Plancque, G.; Moulin, V.; Toulhoat, P.; Moulin, C. Europium Speciation by Time-Resolved Laser-Induced Fluorescence. *Anal. Chim. Acta* **2003**, *478* (1), 11–22.

(48) Piriou, B.; Fedoroff, M.; Jeanjean, J.; Bercis, L. Characterization of the Sorption of Europium(III) on Calcite by Site-Selective and Time-Resolved Luminescence Spectroscopy. *J. Colloid Interface Sci.* **1997**, *194*, 440–447.

(49) Marques Fernandes, M.; Schmidt, M.; Stumpf, T.; Walther, C.; Bosbach, D.; Klenze, R.; Fanghänel, T. Site-Selective Time-Resolved Laser Fluorescence Spectroscopy of Eu3+ in Calcite. *J. Colloid Interface Sci.* **2008**, *321* (2), 323–331.

(50) Bukovská, Z.; Verner, K. *Comprehensive Geological Characterization of URF Bukov, Technical Report No. 247/2018, SURAO*; 2018.

(51) Cho, M.; Fawcett, J. J. Morphologies and Growth Mechanisms of Synthetic Mg-Chlorite and Cordierite. *Am. Mineral.* **1986**, *71*, 78–84.

(52) Grigsby, J. D. Origin and Growth Mechanism of Authigenic Chlorite in Sandstones of the Lower Vicksburg Formation, South Texas. *J. Sediment. Res.* **2001**, *71* (1), 27–36.

(53) Mariano, A. N.; Ring, P. J. Europium-Activated Cathodoluminescence in Minerals. *Geochim. Cosmochim. Acta* **1975**, *89*, 649–660.

(54) Allard, B. *Sorption of Actinides in Granitic Rock, Report*; 1982.

(55) Andersson, K.; Torstenfelt, B.; Allard, B. *Sorption of Radionuclides in Geologic Systems, Report*; 1983.

(56) Huber, M.; Halas, S.; Sikorska, M. Evolution of Prehnite–Albite–Calcite Veins in Metamorphic Rocks from the Lapland Granulite Belt (Kandalaksha Region of Kola Peninsula). *Geologija* **2007**, *59* (3), 1–7.

Acknowledgements

We want to thank F. Laufek, Czech Geological Survey, Prague, Czech Republic and Salim Shams, Helmholtz-Zentrum Dresden – Rossendorf, Institute of Resource Ecology, Dresden, Germany for conducting the PXRD measurements and analysis. A part of the activities was funded by Czech Technological Agency under Project No. TH02030543. We gratefully acknowledge funding by the German Federal Ministry of Education and Research (BMBF), grant 02NUK053B and the Helmholtz Association, grant SO-093 (iCross)

Supporting Information

Excerpt of the URF Bukov geology; Batch sorption data and sample preparation; PXRD data; Raman reference spectra; µTRLFS mappings of A1 and A2 of sorption uptake (F_1+F_2) and speciation (F_2/F_1); detailed lifetime data and locations; Representative spectra for the most important non-quenching mineral phases; Delayed spectra of apatite and feldspar

Additional Information

Competing interests: The authors declare no competing interests.

TOC graphic

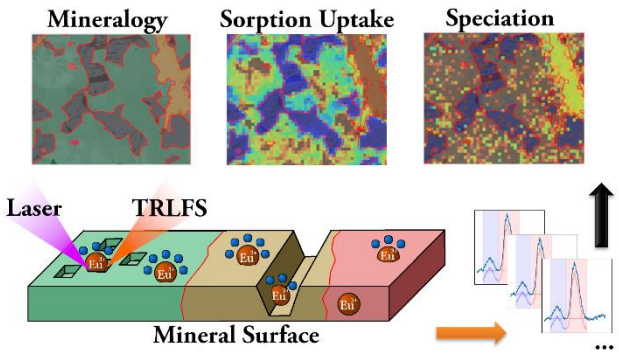

Synopsis: Spatially-resolved spectroscopy revealed the mechanism of uptake of Eu(III) on a complex natural crystalline rock sample.